ARCS22_ 145

ANALYSIS ON THE THEORETICAL PRECISION AND EMPIRICAL ACCURACY OF UNDERWATER OBJECT-TO-IMAGE CORRESPONDENCE IN A FLAT-REFRACTIVE IMAGING SYSTEM

Chun-Kai Wang[1] and Jen-Jer Jaw[2]
[1]Rm. 213, Civil Engineering, National Taiwan University, No. 1, Sec. 4, Roosevelt Rd., Da'an Dist., Taipei 106, Taiwan,
Email: r10521810@ntu.edu.tw
[2]Rm. 208B, Civil Engineering, National Taiwan University, No. 1, Sec. 4, Roosevelt Rd., Da'an Dist., Taipei 106, Taiwan,
Email: jejaw@ntu.edu.tw

KEY WORDS: underwater photogrammetry, flat-refractive imaging system, positioning quality, empirical accuracy, theoretical precision

ABSTRACT: Flat-refractive imaging system, one of the camera geometry of underwater photogrammetry involves the multi-medium environment during the imaging. Accordingly, refraction effect plays an important role in the object-to-image correspondence of flat-refractive imaging system. In order to employ the appropriate specification of the camera system, and support a better implementation when carrying out underwater photogrammetry using flat-refractive imaging system, this study focuses on the positioning quality in object space caused by influential factors through the actual imaging path. Besides, clarifying the sensitivity of parameters in object-to-image correspondence is also a part of research purpose. The parameters related to flat-refractive imaging system discussed in this research include glass thickness, glass distance, and glass interface tilt. The quality assessment is based on the qualitative analysis of the influential factors and equations related to imaging path. To verify the model and the results, the empirical accuracy which is calculated from the projection distance from the object point to the ray traced into the water resulting from erroneous parameters and theoretical precision which is calculated by error propagation are analyzed in this research. With the configuration of this research, the positioning quality is less than or equal to about 10^{-5}m grade when contaminated with 1mm calibrated error of glass thickness is existed, the positioning quality is less than or equal to about $10^{-4}\sim10^{-5}$m grade when 1mm calibrated error of glass distance is existed, and the positioning quality is less than or equal to about 10^{-4}m grade when 1 minute calibrated error of glass interface tilt is existed. According to the results in this research and the users' accuracy requirements, users are able to acquire the maximum value of the acceptable calibrated error for each single influential factor.

1. INTRODUCTION

1.1 Motivation and purpose

The camera geometry of underwater photogrammetry can be of air-to-water and in the water types. The latter can be made by using a waterproof camera or a camera with housing. The imaging system of a camera with glass interface is able to bear deeper water pressure. Housing device facilitates higher quality camera to acquire the images in deeper water. When taking images in the water using a camera with housing, it goes through three mediums, water, glass, and air, along the imaging path. In order to have appropriate object-to-image correspondence in underwater photogrammetric 3D reconstruction, not only are the interior and exterior orientation parameters of images and lens distortion parameters needed, but also the glass interface related parameters, and relationship between glass interface and camera are essential. For example, the glass thickness, the projection distance from the perspective center to the glass surface which is nearest to perspective center (hereinafter to be referred as glass distance), the orientation of the glass interface, etc., as well as the error influence resulting from these factors must be cautiously evaluated.

There are mainly three types of calibration models and methods tackling flat-refractive imaging system using in the water, implicit compensation by other camera parameters, strict ray tracing model, and alternative or virtual camera models (Rofallski and Luhmann, 2022). Not only Fryer and Fraser (1986), Harvey and Shortis (1998) but also Lavest et al. (2000) compensated refraction effect by employing principal distance or lens distortion; Li et al. (1996) and Li et al. (1997) expressed actual path taking the refraction effect into consideration through strict ray tracing model; On the other hand, Telem and Filin (2010) proposed modified model to keep collinearity property. Through the aforementioned studies, it can be seen that refraction effect is of importance when dealing with photogrammetric underwater survey and mapping. Besides, there must be existed error in glass interface and the involved parameters. The error would affect the quality of object-to-image correspondence, thus the positioning results in object space. Yet, to the authors' knowledge, there is still a lack of using the actual imaging path to discuss and analyze the positioning

quality in object space caused by influential factors based on flat-refractive imaging system, and clarifying the sensitivity of parameters in object-to-image correspondence. Therefore, this study aims to fill in the aforementioned missing information to support a better implementation when carrying out underwater photogrammetry using flat-refractive imaging system.

1.2 Influential factors and the terminology

The parameters related to flat-refractive imaging system include the glass thickness, glass distance, glass interface tilt, refractive index, and normal vector of glass interface. Among them, glass interface tilt means the angle of the normal vector of the glass interface relative to the optical axis. The influential factors discussed in this research include glass thickness, glass distance, and glass interface tilt. The terminology related to the object-to-image correspondence in this study is given as follows: (1) piercing point: the intersection point of imaging ray and interface; (2) symmetric point of refraction deformation: intersection point of interface normal vector passing through the perspective center and image plane; (3) imaging variation: the distance between the image points through different influential factors; (4) refraction displacement: the displacement between the image points through pure perspective projection and the one with refraction effect for the same object point.

2. METHODOLOGY

The methodologies in this research include the introduction of object-to-image correspondence taking the refraction effect into consideration, qualitative analysis of the influential factors, equations related to imaging path, and quality assessment.

2.1 Object-to-image correspondence

Figure 1 shows the geometry of object-to-image correspondence of flat-refractive imaging system. The ray starts from the object point and passes through the interface between water and glass. Refraction occurs due to the change of medium and the piercing point is formed on the glass interface which is nearest to object point (hereinafter to be referred as outer interface). After that, another piercing point is formed on the glass interface which is nearest to perspective center (hereinafter to be referred as inner interface) when the ray passes through the interface between glass and air. Then the ray toward the perspective forms an image point on the image plane.

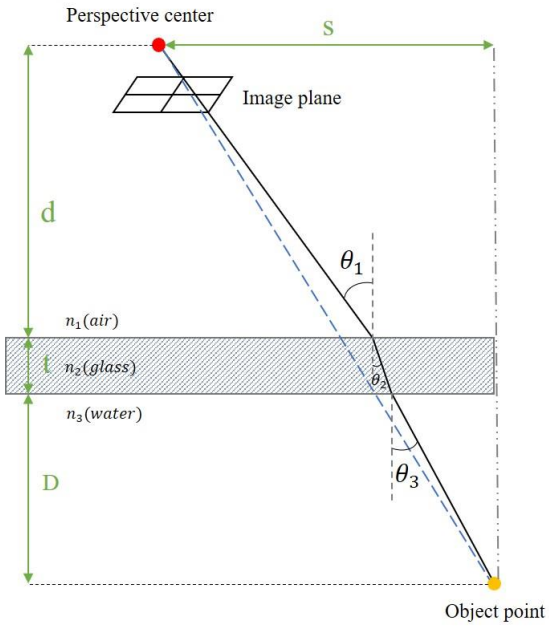

Figure 1. the geometry of object-to-image correspondence (revised from Maas (1995))

2.2 Qualitative Analysis

2.2.1 Influence of the angle of incident ray

Figure 2 shows the geometry of incident rays, the red, green, yellow and blue lines. The pink line means the image plane. The angle of θ_1 is the same as θ_2. Besides, the image point which images by perspective projection is between the image point of yellow line and the image point of blue line. The three points are collinear.
When the angle of incident ray is larger, the distance between the image point and the symmetric point of refraction deformation will be greater. In figure 2, the angle of θ_1 is same as θ_2, but the amounts of difference between image points d_1 is less than d_2. As a result, when the larger the angle of incident ray, the greater the amounts of refractive displacement, and the amounts of difference between image points corresponding the same angle of incident ray is also bigger.

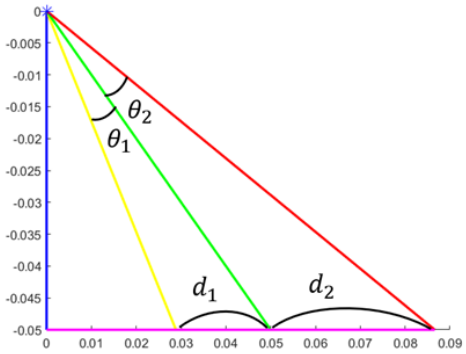

Figure 2. The rays with different angles of incidence

2.2.2 Influence of glass thickness and glass distance

The following is based on the case of without tilt. Figure 1 is expressed by Equation 1, and Equation 1 is constructed by the geometry which is expressed by trigonometric functions and Snell's law. For flat-refractive imaging system, $n_1,\ n_2, n_3$ in Equation 1 means the refractive index of air, glass, water, respectively. Between these refractive index, n_2 is the largest, and n_1 is the smallest. As a result, $\frac{n_1}{n_2}$ and $\frac{n_1}{n_3}$ are all less than 1. Besides, in the case of discussing the same object point, the sum of d, t, and D is fixed. The range of angle of the incident ray is between 0° to 90°, the sine function with an angle of 0° to 90° corresponds to a value of 0 to 1, and the values corresponding to the tangent function from 0° to 90° will be incremented from smallest to largest and both will be greater than 0. In Equation 1, let "$tan(\theta_1)$" is "α", "$tan\,(sin^{-1}(\frac{n_1}{n_2} \times sin(\theta_1)))$" is "β", and "$tan\,(sin^{-1}(\frac{n_1}{n_3} \times sin(\theta_1)))$" is "γ". Because of $\frac{n_1}{n_2}$ is less than $\frac{n_1}{n_3}$, $\alpha > \gamma > \beta$.
Based on the aforementioned, three properties can be acquired by Equation 1 as follow: (1) when d is fixed, if t increases, D decreases, and θ_1 should increase to satisfy the Equation 1; (2) when t is fixed, if d increases, D decreases, and θ_1 should decrease to satisfy the Equation 1; (3) when t is fixed, the change in θ_1 caused by the increase or decrease of d is greater than t. The trend of increase or decrease of θ_1 in Figure 1 will be the same as that of θ_3, and θ_3 is related the ray direction in object space. As a result, the influence of d on imaging and the ray in the object space is greater than t.
The discussion is based on two different object points which object distance are different, but the X and Y coordinates are the same (in the case that Z axis is the direction along the object distance and the plane composed of X axis and the Y axis is parallel to the image plane and the interface) with same configuration (same d and t, but there is without glass interface tilt). Therefore, there are different D, and the property can be acquired by Equation 1 as follow: (4) when t and d are all fixed, if D increases, θ_1 should increase to satisfy the Equation 1.

$$d \times tan(\theta_1) + t \times tan\,(sin^{-1}(\frac{n_1}{n_2} \times sin(\theta_1))) + D \times tan\,(sin^{-1}(\frac{n_1}{n_3} \times sin(\theta_1))) = s \quad (1)$$

2.2.3 Influence of glass interface tilt

Derived from Figure 1, when the normal vector of optical axis is same as the configuration in Figure 1 and tilt the glass interface. At this time, the normal vector of these planes are different. The discussion is based on two different object points which object distance are different, but the X and Y coordinates are the same (in the case that Z axis is the direction along the object distance and the plane composed of X axis and the Y axis is parallel to the image plane and the interface) with same configuration (same d and t, but there is without glass interface tilt). Two unparallel rays are assumed. When the longer the length of the two unparallel rays, the farther between the two rays. The angle between the two unparallel rays is same as the glass interface tilt discussed in this research. Therefore, the

aforementioned object points with larger object distance, the calibrated error of glass interface tilt has greater impact on the ray in the object space.

2.3 Equations of flat-refractive imaging path

Based on the two-medium ray tracing used in air-to-water type (Lee, 2018), the ray tracing of flat-refractive imaging system is derived in this research. In order to reconstruct the trajectory of ray, the parameters related to the glass interface (including glass thickness, glass distance, glass interface tilt), refractive index of all mediums, normal vector of image plane and interface, interior and exterior orientation parameters are given by simulation. After that, the piercing points can be calculated by iteration. The method is called ray tracing. The configuration of object points is same as the lattice points, and three-dimensional coordinates of the object points are $(\mathrm{X_A}, Y_A, Z_A)$. The three-dimensional coordinate of perspective center is $(\mathrm{X_L}, Y_L, Z_L)$. The three-dimensional coordinates of the piercing point on the inner interface $(\mathrm{X_{P_1}}, Y_{\mathrm{P_1}}, Z_{\mathrm{P_1}})$ and the piercing point on the outer interface $(\mathrm{X_{P_2}}, Y_{\mathrm{P_2}}, Z_{\mathrm{P_2}})$ are derived from the object points and perspective center.

Two plane equation of glass interface is given, and the normal vector of the plane $\vec{N}$ are known. Assume the planes are parallel, two normal vectors are the same. The incident vector $\vec{u} = (\mathrm{X_{P_1}} - \mathrm{X}_L, Y_{\mathrm{P_1}} - Y_L, Z_{\mathrm{P_1}} - Z_L)$ is composed of perspective center and the piercing point on the inner interface. Through inner product formula, incident angle of ray θ_a is calculated by $\vec{u}$ and $\vec{N}$. As shown in Equation 2.

$$\theta_a = \cos^{-1}\left(\frac{-\vec{u}\cdot\vec{N}}{|\vec{u}||\vec{N}|}\right) \tag{2}$$

As shown in Equation 3, through Snell's law, the angle of refraction θ_g is formed by the ray deflecting when it travels through the interface.

$$\theta_g = \sin^{-1}(\sin\theta_a * \frac{n_a}{n_g}) \tag{3}$$

Where n_a: refractive index of air; n_g: refractive index of glass

Through the cross product, unit rotation axis $\overrightarrow{\mathrm{k_1}} = [\alpha_1, \beta_1, \gamma_1]$ is generated by $\vec{u}$ and $\vec{N}$, as shown in Equation 4.

$$\overrightarrow{\mathrm{k_1}} = [\alpha_1, \beta_1, \gamma_1] = \frac{\vec{u}\times\vec{N}}{|\vec{u}\times\vec{N}|} \tag{4}$$

Rotation angle θ_1 is the difference between θ_a and θ_g, as shown in Equation 5. Rotation matrix $\mathrm{M_1}'$ is composed of $\overrightarrow{\mathrm{k_1}}$ and θ_1. In order to acquire the unit vector of refraction $\vec{v}$, $\vec{u}$ is rotated by $\mathrm{M_1}'$, as shown in Equation 6.

$$\theta_1 = \theta_a - \theta_g \tag{5}$$

$$\vec{v} = \mathrm{M_1}' * \vec{u} \tag{6}$$

Where

$$\mathrm{M_1}' = \begin{bmatrix} \alpha^2(1-\cos\theta_1)+\cos\theta_1 & \alpha\beta(1-\cos\theta_1)-\gamma\sin\theta_1 & \alpha\gamma(1-\cos\theta_1)+\beta\sin\theta_1 \\ \alpha\beta(1-\cos\theta_1)+\gamma\sin\theta_1 & \beta^2(1-\cos\theta_1)+\cos\theta_1 & \beta\gamma(1-\cos\theta_1)-\alpha\sin\theta_1 \\ \alpha\gamma(1-\cos\theta_1)-\beta\sin\theta_1 & \beta\gamma(1-\cos\theta_1)+\alpha\sin\theta_1 & \gamma^2(1-\cos\theta_1)+\cos\theta_1 \end{bmatrix}$$

Equation 6 can also be expressed as Equation 7.

$$\begin{bmatrix} \mathrm{X_{P_2}} - \mathrm{X_{P_1}} \\ Y_{\mathrm{P_2}} - Y_{\mathrm{P_1}} \\ Z_{\mathrm{P_2}} - Z_{\mathrm{P_1}} \end{bmatrix} = \mathrm{M_1}' * \begin{bmatrix} \mathrm{X_{P_1}} - \mathrm{X}_L \\ Y_{\mathrm{P_1}} - Y_L \\ Z_{\mathrm{P_1}} - Z_L \end{bmatrix} \tag{7}$$

The incident vector of the second refraction is the same as the vector of refraction of the first refraction, and the incident angle of the second refraction is the same as the angle of refraction of the first refraction. Hence, the incident angle of the second refraction is θ_g. As shown in Equation 8, through Snell's law, the angle of refraction θ_w is formed

by the ray deflecting when it travels through the interface.

$$\theta_w = \sin^{-1}\left(\sin\theta_a * \frac{n_a}{n_w}\right) \tag{8}$$

Where n_w: refractive index of water

Through the cross product, unit rotation axis$\overrightarrow{\mathrm{k}_2} = [\alpha_2, \beta_2, \gamma_2]$ is generated by $\vec{v}$ and $\vec{N}$, as shown in Equation 9.

$$\overrightarrow{\mathrm{k}_2} = [\alpha_2, \beta_2, \gamma_2] = \frac{\vec{v} \times \vec{N}}{\left|\vec{v} \times \vec{N}\right|} \tag{9}$$

Rotation angle θ_2 is the difference between θ_g and θ_w, as shown in Equation 10. Rotation matrix $\mathrm{M_2}'$ is composed of $\overrightarrow{\mathrm{k}_2}$ and θ_2. In order to acquire the unit vector of refraction $\vec{w}$, $\vec{v}$ is rotated by $\mathrm{M_2}'$, as shown in Equation 11.

$$\theta_2 = \theta_g - \theta_w \tag{10}$$
$$\vec{w} = \mathrm{M_2}' * \vec{v} \tag{11}$$

Where

$$\mathrm{M_2}' = \begin{bmatrix} \alpha^2(1-\cos\theta_2)+\cos\theta_2 & \alpha\beta(1-\cos\theta_2)-\gamma\sin\theta_2 & \alpha\gamma(1-\cos\theta_2)+\beta\sin\theta_2 \\ \alpha\beta(1-\cos\theta_2)+\gamma\sin\theta_2 & \beta^2(1-\cos\theta_2)+\cos\theta_2 & \beta\gamma(1-\cos\theta_2)-\alpha\sin\theta_2 \\ \alpha\gamma(1-\cos\theta_2)-\beta\sin\theta_2 & \beta\gamma(1-\cos\theta_2)+\alpha\sin\theta_2 & \gamma^2(1-\cos\theta_2)+\cos\theta_2 \end{bmatrix}$$

Equation 11 can also be expressed as Equation 12.

$$\begin{bmatrix} \mathrm{X}_A - \mathrm{X}_{\mathrm{P}_2} \\ Y_A - Y_{\mathrm{P}_2} \\ Z_A - Z_{\mathrm{P}_2} \end{bmatrix} = \mathrm{M_2}' * \begin{bmatrix} \mathrm{X}_{\mathrm{P}_2} - \mathrm{X}_{\mathrm{P}_1} \\ Y_{\mathrm{P}_2} - Y_{\mathrm{P}_1} \\ Z_{\mathrm{P}_2} - Z_{\mathrm{P}_1} \end{bmatrix} \tag{12}$$

Through using given configuration and complete ray tracing path and assuming the coordinate of piercing point on inner interface as unknown parameter, Equation 13 expresses that starting from the coordinates of piercing point on inner interface, the coordinates of true value of the object point should be acquired according to the above process. The piercing point on inner interface can be calculated by iteration to satisfy Equation 13. The image point coordinate can be calculated based on the collinearity properties of perspective center, image point, and piercing point on inner interface. The threshold of stopping iteration is that the distance between the image point calculated this time and last time is less than subpixel (subpixel is 5.5×10^{-7}m in experiment).

$$\left(\begin{bmatrix} \mathrm{X}_{\mathrm{P}_1} \\ Y_{\mathrm{P}_1} \\ Z_{\mathrm{P}_1} \end{bmatrix} + \begin{bmatrix} X_{\vec{v}} & X_{\vec{w}} \\ Y_{\vec{v}} & Y_{\vec{w}} \\ Z_{\vec{v}} & Z_{\vec{w}} \end{bmatrix} \begin{bmatrix} s_1 \\ s_2 \end{bmatrix}\right) - \begin{bmatrix} \mathrm{X}_A \\ Y_A \\ Z_A \end{bmatrix} = 0 \tag{13}$$

Where $s_1 = \frac{t}{\cos\theta_g}$; $s_2 = \frac{D}{\cos\theta_w}$

2.4 Positioning quality assessment in object space

The analysis of positioning quality in object space includes empirical accuracy and theoretical precision.

2.4.1 Empirical accuracy

According to subsection 2.3, following the imaging path, the coordinates of image points are calculated with the configured parameters and three-dimensional coordinates of the object points. The coordinates of image points are regarded as ground truth data. Accordingly, the projection distance from the object point to the ray traced into the water resulting from erroneous parameters can be then determined to serve as the positioning quality, also the empirical accuracy, in the object space, as shown in Figure 3. This method uses a single image to analyze the positioning quality in object space. Compared with utilizing intersection computation of pair images, the way conducted by a single image can be more convenient to the analysis of positioning quality for each individual factor.

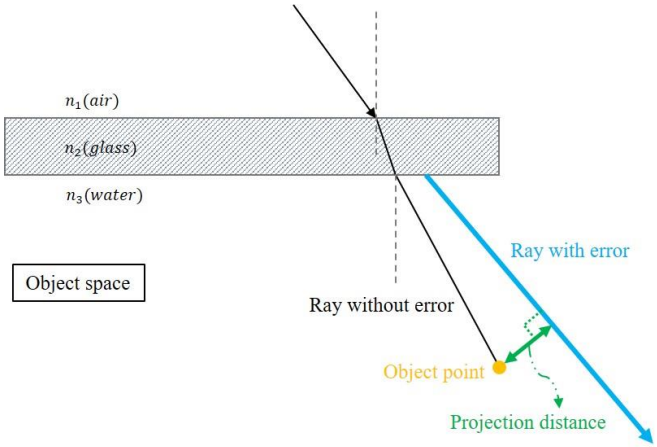

Figure 3. Distance between true value of the object point and projection point

2.4.2 Theoretical precision

The standard deviations of the projection point can be treated as the theoretical precision of positioning quality. And it can be attained by applying error propagation into the imaging path. As shown in Equation 14, the observation function of the coordinates of projection points is conducted through error propagation taking influential factors into consideration.

$$\Sigma_{\text{ProjectionPoint}} = \begin{bmatrix} {\sigma_X}^2 & \sigma_{XY} & \sigma_{XZ} \\ \sigma_{YX} & {\sigma_Y}^2 & \sigma_{YZ} \\ \sigma_{ZX} & \sigma_{ZY} & {\sigma_Z}^2 \end{bmatrix} = \left(\frac{\partial \mathrm{F}}{\partial \xi}\right) \Sigma_{\xi} \left(\frac{\partial \mathrm{F}}{\partial \xi}\right)^T \tag{14}$$

Where ξ: influential factor; Σ_{ξ}: variance of influential factor;
F: the observation function of the coordinates of projection points;
$\Sigma_{\text{ProjectionPoint}}$: variance − covariance matrix of the coordinates of projection points (X, Y, Z)

3. EXPERIMENTS AND RESULTS

The true value of the object points and configuration which are given by means of simulation, in order to acquire the positioning error when the influential factors related to the flat-refractive imaging system with the calibrated error at different location of object points. According to the methodology written in section 2, the empirical accuracy and theoretical precision of positioning quality in object space can be calculated and the experimental results are integrated to each interval.

3.1 Experimental configuration

The data used in experiment are given by means of simulation. Among them, Some parameters and configuration are referred to the study of Rofallski and Luhmann (2022). Table 1 shows camera specification, interior and exterior orientation parameters, the parameters related to flat-refractive imaging system, and refractive index. As shown in Figure 4, 243 object points are given by means of simulation, both the X and Y components are simulated every 0.375m from -1.5m to 1.5m, Z component (direction of object distance) is simulated every 1m from -2m to -4m.

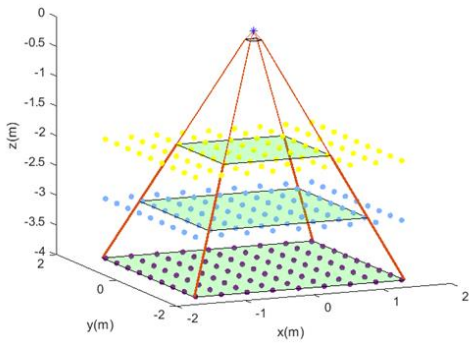

Figure 4. Object points

Table 1. Configuration and parameters

Configuration and parameters	Content or value
Camera	acA2040-25gm - Basler ace (Rofallski and Luhmann, 2022)
Resolution	2048px × 2048px (Rofallski and Luhmann, 2022)
Sensor size	11.3mm × 11.3mm (Rofallski and Luhmann, 2022)
Pixel size	5.5µm × 5.5µm (Rofallski and Luhmann, 2022)
Principal point	(0, 0)
Principal distance	10mm (Rofallski and Luhmann, 2022)
Perspective center	(0, 0, 0)
Rotations around the 3 axes	(0°, 0°, 0°)
Glass thickness	2mm~10mm
Glass distance	3cm~15cm
Refractive index of glass	1.49 (Rofallski and Luhmann, 2022)
Refractive index of air	1.00028 (Rofallski and Luhmann, 2022)
Refractive index of water	1.33 (Rofallski and Luhmann, 2022)

3.2 Experimental results

Based on the properties in subsection 2.2.1, subsection 2.2.2 (1), and subsection 2.2.2 (1), the experimental results will present the security value of the influence of positioning in object space corresponded to the calibrated error per unit of each influential factors. Subsections 2.2.2 (3) and (4) and Subsection 2.2.3 are verified in Subsection 3.2 by quantitative analysis and the values can be acquired.

3.2.1 Interpretation of experiment

Figure 5 shows the distance between each true value of the object point which object distance is 2m and its projection point. This subsection uses Figure 5 which shows empirical accuracy as an example for interpretation. Based on the properties in subsection 2.2.1, subsection 2.2.2 (1), and subsection 2.2.2 (1), using the image points which are regarded as ground truth data and the glass with 1 mm difference in thickness from the original configuration, the projection distance from the object point to the ray traced into the water resulting from erroneous parameters can be calculated and determined to serve as the positioning quality. After the calculation, Figure 5 can be acquired by interpolation and Table 2 can be integrated from Figure 5. The “error” in Table 2 means ”The error corresponds to the coordinate interval in object space”.
If an object point which object distance is 2m and the absolute value of the X and Y coordinates is less than or equal to 0.5m, when 1mm calibrated error of glass thickness is existed, security value of the influence of positioning in object space is between $0\sim4.1\times10^{-5}$m in Figure 5. Table 3, Table 4, and Table 5 are all generated and interpreted in the same way.

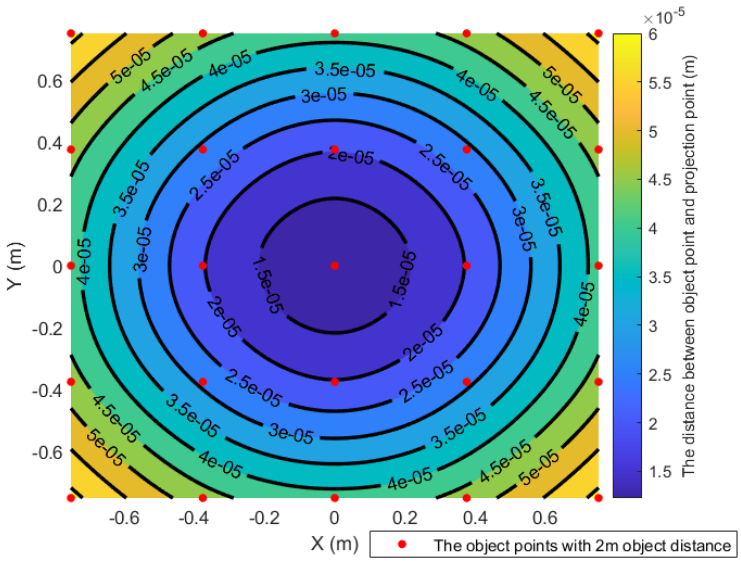

Figure 5. The positioning quality in object space when 1mm calibrated error of glass thickness is existed for the object point which object distance is 2m (empirical accuracy)

Table 2. The positioning quality in object space when 1mm calibrated error of glass thickness is existed for the object point which object distance is 2m

Object distance		2m
error	$(\|X\| \le 0.5\text{m}, \|Y\| \le 0.5\text{m})$	$0\sim4.1\times10^{-5}\text{m}$
	$(0.5\text{m} \le \|X\| \le 1\text{m}, 0.5\text{m} \le \|Y\| \le 1\text{m})$	$(0.5\text{m} \le \|X\| \le 0.75\text{m}, 0.5\text{m} \le \|Y\| \le 0.75\text{m})$：$4.1\times10^{-5}\sim6.2\times10^{-5}\text{m}$
		$(0.75\text{m} \le \|X\| \le 1\text{m}, 0.75\text{m} \le \|Y\| \le 1\text{m})$：Object point is not imaged on the image plane
	$(1\text{m} \le \|X\| \le 1.5\text{m}, 1\text{m} \le \|Y\| \le 1.5\text{m})$	Object point is not imaged on the image plane

3.2.2 The positioning quality in object space

Table 3, Table 4, and Table 5 shows the positioning quality in object space when 1mm calibrated error of glass thickness is existed, 1mm calibrated error of glass distance is existed, and 1minute calibrated error of glass interface tilt is existed, respectively. The "error" in Table 3, Table 4, and Table 5 all mean "The error corresponds to the coordinate interval in object space". The empirical accuracy is shown before the slash and theoretical precision is shown after the slash in Table 3, Table 4, and Table 5. When the glass interface tilt increases, although some object points are located in the intervals listed in the table, they are not suitable for this table if they are not imaged on the image plane.

Table 3. The positioning quality in object space when 1mm calibrated error of glass thickness is existed

Object distance		2m	3m	4m
error	$(\|X\| \le 0.5\text{m}, \|Y\| \le 0.5\text{m})$	$0\sim4.1\times10^{-5}\text{m}/0\sim4.1\times10^{-5}\text{m}$	$0\sim2.7\times10^{-5}\text{m}/0\sim2.7\times10^{-5}\text{m}$	$0\sim2.0\times10^{-5}\text{m}/0\sim2.0\times10^{-5}\text{m}$
	$(0.5\text{m} \le \|X\| \le 1\text{m}, 0.5\text{m} \le \|Y\| \le 1\text{m})$	$(0.5\text{m} \le \|X\| \le 0.75\text{m}, 0.5\text{m} \le \|Y\| \le 0.75\text{m})$：$4.1\times10^{-5}\sim6.2\times10^{-5}\text{m}/4.1\times10^{-5}\sim6.2\times10^{-5}\text{m}$	$2.7\times10^{-5}\sim5.7\times10^{-5}\text{m}/2.7\times10^{-5}\sim5.6\times10^{-5}\text{m}$	$2.0\times10^{-5}\sim4.0\times10^{-5}\text{m}/2.0\times10^{-5}\sim4.0\times10^{-5}\text{m}$
		$(0.75\text{m} \le \|X\| \le 1\text{m}, 0.75\text{m} \le \|Y\| \le 1\text{m})$：Object points are not imaged on the image plane		
	$(1\text{m} \le \|X\| \le 1.5\text{m}, 1\text{m} \le \|Y\| \le 1.5\text{m})$	Object points are not imaged on the image plane	$(1\text{m} \le \|X\| \le 1.125\text{m}, 1\text{m} \le \|Y\| \le 1.125\text{m})$：$5.7\times10^{-5}\sim6.2\times10^{-5}\text{m}/5.6\times10^{-5}\sim6.2\times10^{-5}\text{m}$	$4.0\times10^{-5}\sim6.2\times10^{-5}\text{m}/4.0\times10^{-5}\sim6.2\times10^{-5}\text{m}$
			$(1.125\text{m} \le \|X\| \le 1.5\text{m}, 1.125\text{m} \le \|Y\| \le 1.5\text{m})$：Object points are not imaged on the image plane	

Table 4. The positioning quality in object space when 1mm calibrated error of glass distance is existed

Object distance		2m	3m	4m
error	$(\|X\| \le 0.5\text{m}, \|Y\| \le 0.5\text{m})$	$0\sim1.38\times10^{-4}\text{m}/0\sim1.38\times10^{-4}\text{m}$	$0\sim8.4\times10^{-5}\text{m}/0\sim8.4\times10^{-5}\text{m}$	$0\sim6.0\times10^{-5}\text{m}/0\sim6.0\times10^{-5}\text{m}$
	$(0.5\text{m} \le \|X\| \le 1\text{m}, 0.5\text{m} \le \|Y\| \le 1\text{m})$	$(0.5\text{m} \le \|X\| \le 0.75\text{m}, 0.5\text{m} \le \|Y\| \le 0.75\text{m})$：$1.38\times10^{-4}\sim2.33\times10^{-4}\text{m}/$	$8.4\times10^{-5}\sim2.04\times10^{-4}\text{m}/8.4\times10^{-5}\sim2.04\times10^{-4}\text{m}$	$6.0\times10^{-5}\sim1.35\times10^{-4}\text{m}/6.0\times10^{-5}\sim1.35\times10^{-4}\text{m}$

		1.38×10^{-4}~2.33×10^{-4}m		
		($0.75\text{m} \leq \lvert X \rvert \leq 1\text{m}$, $0.75\text{m} \leq \lvert Y \rvert \leq 1\text{m}$) : Object points are not imaged on the image plane		
	($1\text{m} \leq \lvert X \rvert \leq 1.5\text{m}$, $1\text{m} \leq \lvert Y \rvert \leq 1.5\text{m}$)	Object points are not imaged on the image plane	($1\text{m} \leq \lvert X \rvert \leq 1.125\text{m}$, $1\text{m} \leq \lvert Y \rvert \leq 1.125\text{m}$) : 2.04×10^{-4}~2.34×10^{-4}m/ 2.04×10^{-4}~2.34×10^{-4}m	1.35×10^{-4}~2.34×10^{-4}m/ 1.35×10^{-4}~2.34×10^{-4}m
			($1.125\text{m} \leq \lvert X \rvert \leq 1.5\text{m}$, $1.125\text{m} \leq \lvert Y \rvert \leq 1.5\text{m}$) : Object points are not imaged on the image plane	

Table 5. The positioning quality in object space when 1minute calibrated error of glass interface tilt is existed

Object distance		2m	3m	4m
error	($\lvert X \rvert \leq 0.5\text{m}$, $\lvert Y \rvert \leq 0.5\text{m}$)	0~1.70×10^{-4}m/ 0~1.70×10^{-4}m	0~2.32×10^{-4}m/ 0~2.32×10^{-4}m	0~3.00×10^{-4}m/ 0~3.00×10^{-4}m
	($0.5\text{m} \leq \lvert X \rvert \leq 1\text{m}$, $0.5\text{m} \leq \lvert Y \rvert \leq 1\text{m}$)	($0.5\text{m} \leq \lvert X \rvert \leq 0.75\text{m}$, $0.5\text{m} \leq \lvert Y \rvert \leq 0.75\text{m}$) : 1.70×10^{-4}~2.04×10^{-4}m/ 1.70×10^{-4}~2.04×10^{-4}m	2.32×10^{-4}~2.94×10^{-4}m/ 2.32×10^{-4}~2.94×10^{-4}m	3.00×10^{-4}~3.40×10^{-4}m/ 3.00×10^{-4}~3.40×10^{-4}m
		($0.75\text{m} \leq \lvert X \rvert \leq 1\text{m}$, $0.75\text{m} \leq \lvert Y \rvert \leq 1\text{m}$) : Object points are not imaged on the image plane		
	($1\text{m} \leq \lvert X \rvert \leq 1.5\text{m}$, $1\text{m} \leq \lvert Y \rvert \leq 1.5\text{m}$)	Object points are not imaged on the image plane	($1\text{m} \leq \lvert X \rvert \leq 1.125\text{m}$, $1\text{m} \leq \lvert Y \rvert \leq 1.125\text{m}$) : 2.94×10^{-4}~3.07×10^{-4}m/ 2.94×10^{-4}~3.07×10^{-4}m	3.40×10^{-4}~4.11×10^{-4}m/ 3.40×10^{-4}~4.11×10^{-4}m
			($1.125\text{m} \leq \lvert X \rvert \leq 1.5\text{m}$, $1.125\text{m} \leq \lvert Y \rvert \leq 1.5\text{m}$) : Object points are not imaged on the image plane	

4. CONCLUSION

This study focuses on the analysis of individual factors. Therefore, this section analyzes the result based on this principle. With the limitation of decimal places shown in Table 3, Table 4, and Table 5, the empirical accuracy is almost the same as the theoretical precision. There are different between empirical accuracy and theoretical precision when the table shown without the limitation of decimal places, but it is enough to say that the empirical accuracy is similar to the theoretical. The reasonableness of model has been verified through the results. Users are able to acquire the maximum value of the acceptable calibrated error for each single influential factor.

Glass thickness: The positioning quality is less than or equal to about 10^{-5}m grade when 1mm calibrated error of glass thickness is existed with the configuration of this research, in object space. The detailed values are shown in Table 3. Based on the same calibrated error of glass thickness, there are two different object points located on the same line along to the object distance. The shorter the object distance, the larger the positioning quality in object space. In the configuration of this research, the detailed values are also shown in Table 3. Based on the result above, the subsection 2.2.2 (4) is verified.

Glass distance: The positioning quality is less than or equal to about 10^{-4}~10^{-5}m grade when 1mm calibrated error of glass distance is existed with the configuration of this research, in object space. The detailed values are shown in Table 4. The positioning quality in object space when calibrated error of glass thickness per unit is existed is larger than glass thickness. Hence, the subsection 2.2.2 (3) is verified and the sensitivity of parameters of glass distance is greater than glass thickness. Based on the same calibrated error of glass thickness, there are two different object points

located on the same line along to the object distance. The shorter the object distance, the larger the positioning quality in object space. In the configuration of this research, the detailed values are also shown in Table 3. Based on the result above, the subsection 2.2.2 (4) is verified.

Glass interface tilt: The positioning quality is less than or equal to about 10^{-4}m grade when 1 minute calibrated error of glass interface tilt is existed with the configuration of this research, in object space. The detailed values are shown in Table 5. When object distance is 2m, the positioning quality when 1 minute calibrated error of glass interface tilt is existed is larger than the positioning quality when 1mm calibrated error of glass thickness is existed, and is similar to the positioning quality when 1mm calibrated error of glass distance is existed; When object distance is 3m or 4m, the positioning quality when 1 minute calibrated error of glass interface tilt is existed is larger than the positioning quality when 1mm calibrated error of glass thickness or glass distance is existed. Based on the same calibrated error of glass thickness, there are two different object points located on the same line along to the object distance. The longer the object distance, the larger the positioning quality in object space. In the configuration of this research, the detailed values are also shown in Table 5. Based on the result above, the subsection 2.2.3 is verified.

Besides, in the case of that Z axis is the direction along the object distance and the plane composed of X axis and the Y axis is vertical to Z axis, when object distances of the object points are same, the larger the absolute value of the X and Y coordinates, the larger the positioning quality in object space. In the configuration of this research, the detailed values are also shown in Table 3, Table 4, and Table 5.
In the future, the refractive index can be included in discussion of individual factors. The experiments of combined parameters are to be thoroughly conducted and the positioning quality in qualitative as well as quantitative aspects are analyzed in detail to have more comprehensive discussion on this topic.

5. REFERENCES

Fryer, J. G., Fraser, C., 1986. On the calibration of underwater cameras. The Photogrammetric Record, 12(67), pp. 73-85.

Harvey, E. S., Shortis, M. R., 1998. Calibration stability of an underwater stereo-video system: implications for measurement accuracy and precision. Marine Technology Society Journal, 32(2), pp. 3-17.

Lavest, J. M., Rives, G., Lapresté, J. T., 2000. Underwater camera calibration. In: European Conference on Computer Vision. Springer, Berlin, Heidelberg, pp. 654-668.

Lee, K. C., 2018. Solving water surface and underwater object points through optical frame imagery. Master thesis, National Taiwan University, Taipei.

Li, R., Tao, C., Zou, W., Smith, R. G., Curran, T. A., 1996. An underwater digital photogrammetric system for fishery geomatics. International Archives of Photogrammetry and Remote Sensing, 31, pp. 319-323.

Li, R., Li, H., Zou, W., Smith, R. G., & Curran, T. A., 1997. Quantitative photogrammetric analysis of digital underwater video imagery. IEEE Journal of Oceanic Engineering, 22(2), pp. 364-375.

Maas, H. G., 1995. New developments in multimedia photogrammetry. Optical 3D measurement techniques III.

Rofallski, R., Luhmann, T., 2022. An Efficient Solution to Ray Tracing Problems in Multimedia Photogrammetry for Flat Refractive Interfaces. PFG–Journal of Photogrammetry, Remote Sensing and Geoinformation Science, pp. 1-18.

Telem, G., & Filin, S., 2010. Photogrammetric modeling of underwater environments. ISPRS Journal of Photogrammetry and Remote Sensing, 65(5), pp. 433-444.